

Document downloaded from:

<http://hdl.handle.net/10251/125677>

This paper must be cited as:

Zaragoza, R.J.; Aurell, M.J.; González-Cardenete, M.A. (2018). A theoretical study on NHC-catalysed enantioselective cycloaddition of ketenes and 3-aryl coumarins: mechanism and enantioselectivity. *Organic & Biomolecular Chemistry*. 16(30):5474-5482.
<https://doi.org/10.1039/c8ob01035h>



The final publication is available at

<http://doi.org/10.1039/c8ob01035h>

Copyright The Royal Society of Chemistry

Additional Information

Theoretical study on NHC-catalysed enantioselective cycloaddition of ketenes and 3-aryl coumarins: Mechanism and enantioselectivity.

Received 00th January 20xx,
Accepted 00th January 20xx

DOI: 10.1039/x0xx00000x

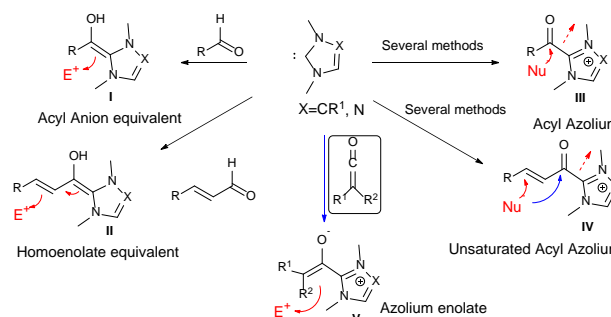
www.rsc.org/

Ramón J. Zaragoza,^{*a} María J. Aurell,^{*a} and Miguel A. González-Cardenete^b

The NHC-catalysed enantioselective cycloaddition of ketenes to 3-aryl coumarins to yield dihydrocoumarin-fused dihydropyranones has been investigated using DFT methods at the B3LYP/6-31G* and MPWB1K/6-311G** computational levels. Two plausible mechanisms have been studied: the “ketene-first” mechanism A and the “coumarin-first” mechanism B. An analysis of the activation Gibbs free energies involved in the two competitive pathways makes it possible to rule out the pathway associated with the “coumarin-first” mechanism B. The first step of the “ketene-first” mechanism A is the formation of zwitterionic intermediate IN1-Z via nucleophilic attack of NHC 1 to ketene 2. [4+2] cycloaddition through nucleophilic attack of enolate IN1-Z to the conjugate double bond of benzoyl group of the coumarin 3, via TS3-SS-a2 or TS3-RR-a2, yield IN3. Finally the extrusion of catalyst through TS5 leads to the final products either 4-SS or 4-RR. The origin of the enantioselectivity observed in the experimental results is determined in the transition states TS3-SS-a2/TS3-RR-a2. In this path, the intramolecular hydrogen-bonding between the hydroxyl group of the IN1-Z adduct and the carbonyl oxygen of the original ketene group directs the final stereochemistry throughout the entire process.

1-Introduction

In recent years, N-heterocyclic carbenes (NHCs) have been successfully utilised as catalysts in organocatalytic reactions.^{1,2} Catalysis in organic chemistry not only makes an acceleration of the reactions possible or improves selectivity but also enables the generation of intermediates distinct from the inherent chemistry of the reagents. The use of N-heterocyclic carbenes (NHCs) has introduced a new set of elementary steps that take place via discrete reactive species, including acyl anion I and homoenolate II equivalents, and acyl azolium III/IV (see Scheme 1). Nearly, all NHC-catalysed reactions proceed at room temperature without the need for stringent exclusion of air and do not generate reaction by-products. Variation of the catalyst, the base, or reaction conditions can profoundly influence reaction outcomes. The use of chiral NHCs has allowed the development of catalysed asymmetric reactions, having made significant progress possible along the past decade.³ Interestingly, while acyl anion I and homoenolate II equivalents are nucleophilic species, allowing the inversion of



Scheme 1 Intermediates generated by reaction of NHCs.

the normal reactivity of the aldehyde precursors, *umpolung* reactivity, acyl azolium cations III and IV are activated electrophilic species with a unique and unprecedented chemistry.¹⁻⁴

The addition of NHCs to ketenes, provides an approach to azolium enolates V (see Scheme 1) that is an alternative to the methods involving rearrangements of acyl anion equivalents. Azolium enolates, generated *in situ* by nucleophilic addition of a N-heterocyclic carbene to an aryl(alkyl)-disubstituted ketene, were employed as dienophiles in [4+2] annulations with enones^{1,5} or benzoyldiazenes,^{1,6} in [2+2] cycloadditions with N-protected imines,^{1,7,8} α -keto aldehydes,¹ diazenedicarboxylates,⁹ benzaldehydes¹⁰ or N-sulfinylanilines,¹ in [3+2] cycloadditions with oxaziridines,¹ in [2+2+2] cycloadditions with isocyanates^{1,11} and in esterification of ketenes.^{1,12}

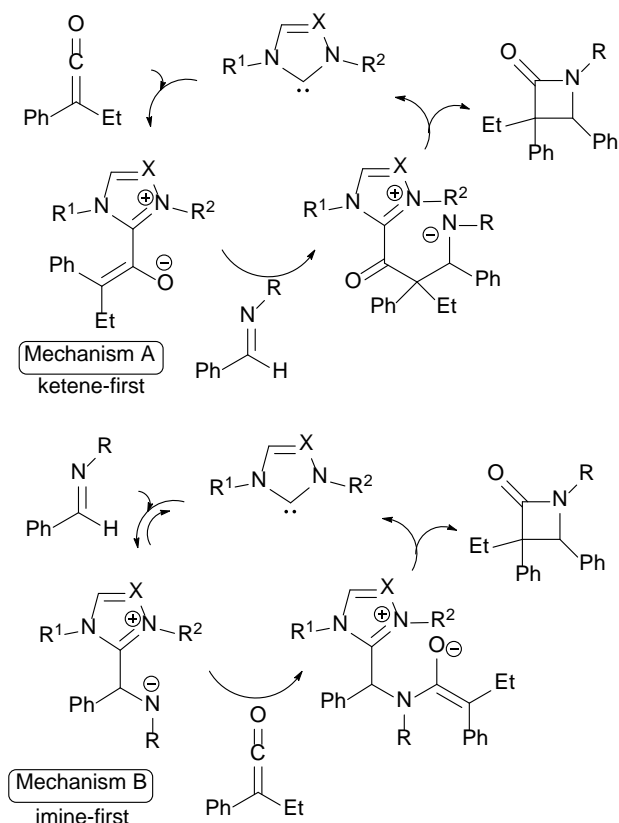
^a Departamento de Química Orgánica, Universidad de Valencia, Dr. Moliner 50, 46100 Burjassot, Valencia, Spain.

^b Instituto de Tecnología Química (UPV-CSIC), Universitat Politècnica de Valencia-Consejo Superior de Investigaciones Científicas, Avda. de los Naranjos s/n, 46022 Valencia, Spain.

E-mail: Ramon.J.Zaragoza@uv.es

† Footnotes relating to the title and/or authors should appear here.

Electronic Supplementary Information (ESI) available: [details of any supplementary information available should be included here]. See DOI: 10.1039/x0xx00000x



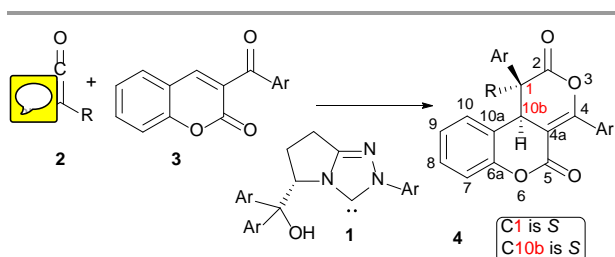
Scheme 2 Two possible catalytic mechanisms in the carbene catalysed Staudinger reaction.

In these types of reactions, it is suggested that the NHC initially reacts with ketene to give the azolium enolate **V**. Then, the enolate **V** reacts with the appropriate species to give the final product (see for example mechanism A in scheme 2).⁴⁻¹⁴ However, Ye and co-workers¹⁵ in the carbene catalysed Staudinger reaction of ketenes with imines suggests two possible mechanisms (Scheme 2). As for denoted “ketene-first” mechanism A, the nucleophilic catalyst initially attacks the ketene to generate a NHC-ketene zwitterionic intermediate, which is followed by reaction between this enolate and the imine to form a second intermediate. Finally, the cyclization of this intermediate to the final β -lactam and expulsion of NHC close the reaction pathway. However, in the “imine-first” mechanism B, the nucleophilic catalyst initially attacks the imine to generate a NHC-imine zwitterionic intermediate. This intermediate attacks to the ketene and after expulsion of NHC

gives the final β -lactam.

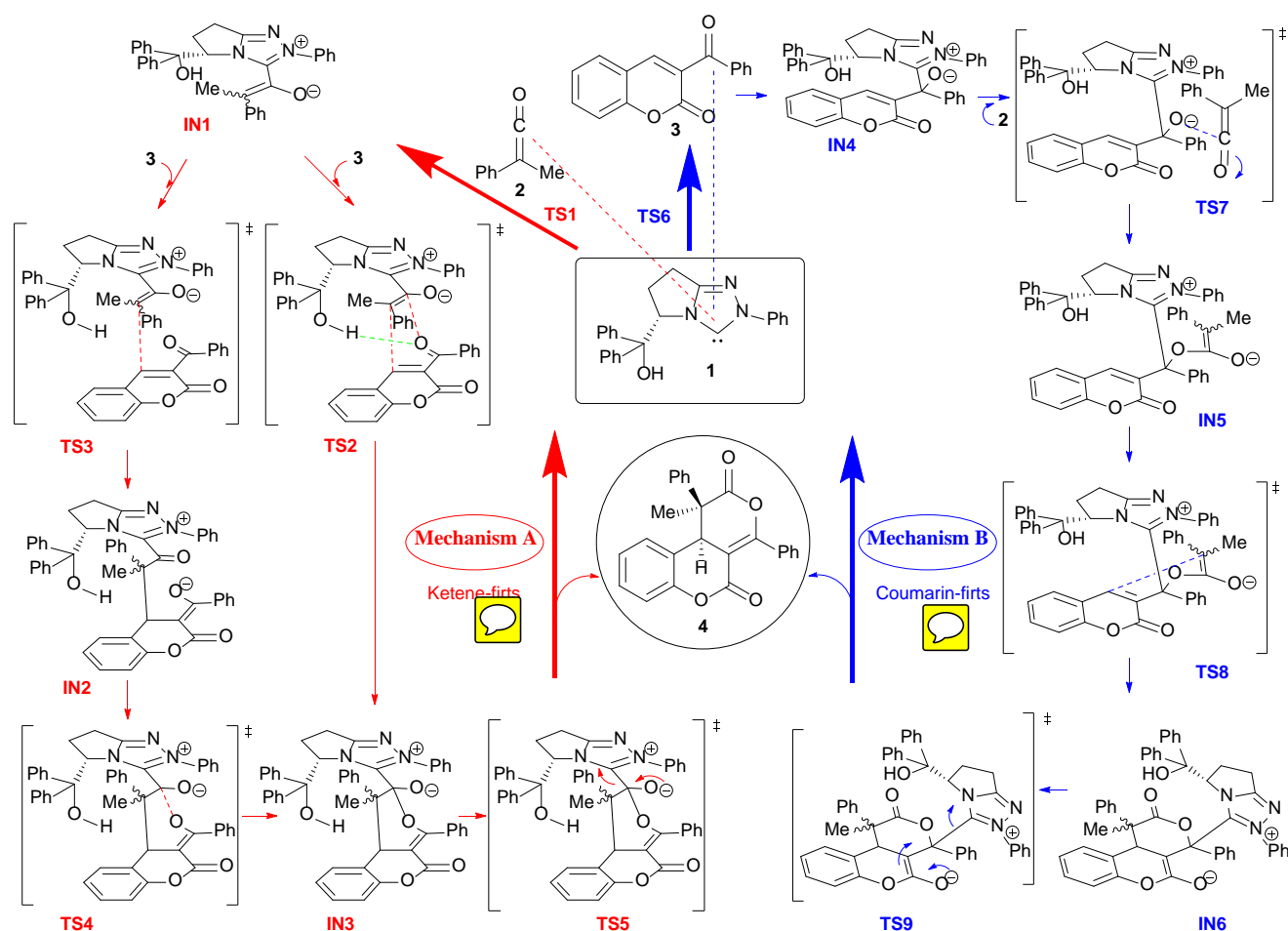
Liu and co-workers¹⁵ performed a DFT study on the two proposed reaction mechanisms¹⁵ and concluded that the “ketene-first” mechanism A is much more feasible than the “imine-first” mechanism B in the NHC-catalysed Staudinger reaction. Subsequently, Tang and co-workers¹⁶ carried out a theoretical investigation toward the [4+2] cycloaddition of ketenes with N-benzoyldiazenes catalysed by NHC and came to the conclusion that in this case the “diazene-first” (similar to the “imine-first” mechanism B) is more favorable than the “ketene-first” mechanism A. Recently, these same authors¹⁷ conducted a theoretical study toward the [4+2] cycloaddition of ketenes with 1-azadienes catalysed by NHC. The calculated results revealed that the “ketene-first” mechanism is more energetically favorable than the “azadiene-first” one (similar to the “imine-first” mechanism B). Recently, Ye and co-workers¹⁸ reported a catalysed [4+2] cycloaddition (using different NHCs, for example **1**) of ketenes **2** and 3-aryl coumarins **3** to give the corresponding dihydrocoumarin-fused multisubstituted dihydropyranones **4** in high yield with high enantioselectivity (Scheme 3). Solvent screening revealed that the reaction performed better in toluene than in DCM or THF in terms of enantioselectivity (42-98% ee). This reaction is very convenient and attractive; however, there are still some questions that need to be solved: a) What is the possible mechanism? : “ketene-first” mechanism A or “coumarin-first” mechanism B, b) What is the possible detailed mechanism? c) Is it possible to predict the final stereochemistry?

Our interest in organocatalysis, more specifically in the participation of NHCs as catalysts,¹⁹ prompted us to perform some DFT studies on the molecular mechanisms of these interesting reactions. Herein, a DFT study for the NHC-catalysed (NHC=**1**, Ar=Ph) reaction of ketene **2** (R=Me) with 3-aryl coumarin **3** (Ar=Ph) yielding dihydrocoumarin-fused dihydropyranones **4** is presented. Two possible mechanisms have been studied, “coumarin-first” or mechanism B and “ketene-first” or mechanism A, and within each one different options have been studied. The “coumarin-first” reaction is totally new and has not been studied to date. Two possible channels have been studied, channel B1 and channel B2. With regard to the second option, “ketene-first” (mechanism A) only the initial step has been studied in similar systems, but the course of such mechanism (subsequent reaction with coumarin) it is the first time it has been studied. Three different mechanistic options, channel A1, channel A2 and channel A3, have been studied. We believe that these computational results should be important for understanding this kind of organocatalytic reaction, and thus provides valuable insights on the rational design for this type of reactions with high enantioselectivity.



Scheme 3 Cycloaddition of ketenes **2** and 3-aryl coumarins **3**.

2- Results and Discussion



Scheme 4 Two proposed reaction channels: the “ketene-first” mechanism A (left in red) and the “coumarin-first” mechanism B (right in blue).

As a computational model we have selected the NHC **1** (Ar=Ph), ketene **2** (R=Me) and 3-aryl coumarin **3** because they construct the simplest reactant structures and also afford relatively high yields and enantiomeric excess values. As shown in Scheme 3, it should be noted that there are two chiral centers (1 and 10b) in the final product **4**, also there are some intermediates with stereocenters or *E/Z* double bonds (see Schemes 4 and 5), so we use letters to represent the chirality (*R/S*) or the stereochemistry (*E/Z*).

The two mechanisms that have been studied are reflected in Scheme 4: “ketene-first” mechanism A and the “coumarin-first” mechanism B. The global mechanistic possibilities are reflected in Scheme 4. Two different mechanisms have been studied: the “ketene-first” mechanism A and the “coumarin-first” mechanism B. In mechanism A, two clearly

differentiated routes have been studied. In the first one, the conversion of intermediate **IN1** to intermediate **IN3** takes place in a single stage through **TS2**. This is the mechanism suggested by Ye and co-workers.¹⁸ In the second route, that conversion takes place through several stages (**TS3** and **TS4**). Firstly, in order to determine which of the two mechanistic possibilities is more reasonable, we will only consider the channels that lead to the mayor enantiomer of **4** (**4-SS**; C1 and C10b with *S* configuration). Later, we will study and compare the routes that lead to both enantiomers (**4-SS** and **4-RR**). The free energy profiles are shown in Fig.1 (see also Tables S1-S6 and Figures S1-S23 of the ESI for a more detail of the energies and geometries of the species involved).

2.1 Computational Methods

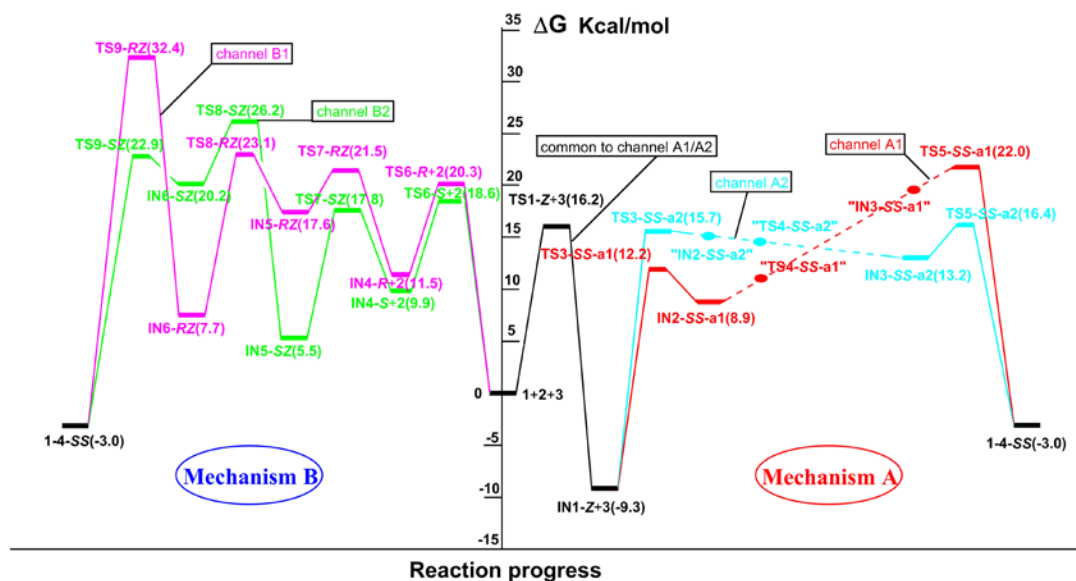


Fig.1 Free energy profiles, at B3LYP/6-31G* level in gas phase, of mechanism A (right) and mechanism B (left). Mechanism A: channel A1 (in red), channel A2 (in blue). Mechanism B: channel B1 (in pink), channel B2 (in green). In dashed line, hypothetical way of reaction. In quotation marks, hypothetical species of reaction.

All calculations were carried out with the Gaussian 09 suite of programs.²⁰ Initially, due to the large size of the molecules, density functional theory²¹ calculations (DFT) have carried out using the B3LYP²² exchange-correlation functionals, together with the standard 6-31G* basis set, in gas phase.²³ For each of the transition states (TS), a careful search has been carried out to locate the most stable conformers.²⁴ In this, the distances, angles and dihedrals involved in the TS have been maintained. The parts of the molecule susceptible to conformational changes have been altered manually. Each of the conformers has been optimized. Only the most stable conformers are presented. The stationary points were characterized by frequency computations in order to verify that transition states have one and only one imaginary frequency. The intrinsic reaction coordinate (IRC) paths²⁵ were traced in order to check the energy profiles connecting each TS to the two associated minima of the proposed mechanisms using the second order González–Schlegel integration method (see Figures S1-S16 of the ESI).²⁵ In the case of problematic IRCs (flat PES in the vicinity of TS), a relaxed scan was performed. The values of enthalpies, entropies and free energies were calculated with the standard statistical thermodynamics at 298.15K and 1 atm.²⁶

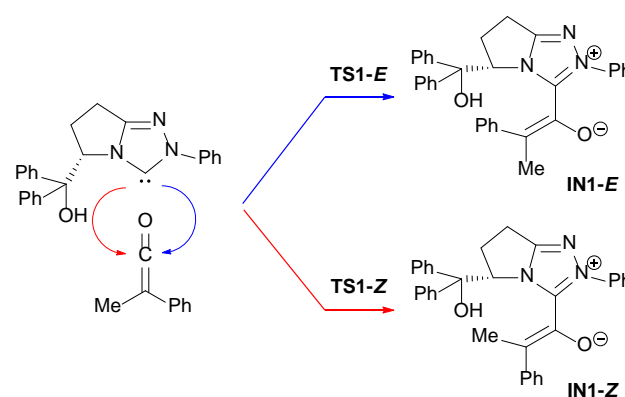
Once the most favorable channels for mechanism A and mechanism B were determined, one-point calculations at MPWB1K/6-311G** level in toluene²⁷ were made of the species involved in these channels. Finally, for the most plausible mechanism, the species involved in this mechanism were totally optimized in toluene, using the MPWB1K hybrid meta functional²⁸ together with the 6-311G** basis set.²⁹ This level of theory has shown to have good results for combinations of thermochemistry and thermochemical kinetics in processes including weak interactions.²⁶ Solvent effects of toluene were taken into account by full optimization using the polarisable

continuum model (PCM) as developed by Tomasi's group²⁷ in the framework of the self-consistent reaction field (SCRF).²⁸

2.2 Mechanism A

The first step of the reaction is the formation of zwitterionic intermediates **IN1-E/IN1-Z** via nucleophilic attack of NHC **1** on both sides of ketene **2** via the transition states **TS1-E/TS1-Z** (Scheme 5). The Gibbs free energy barriers via **TS1-E/TS1-Z** are 19.8 and 17.4 kcal mol⁻¹, respectively (Tables S1-S2 of the ESI), indicating that the Z face attack³⁰ is energetically more favorable than the E face attack in dynamics. Also the following TSs of the pathway have a smaller energy and therefore, it is reasonable to exclude the reaction pathway in the following parts.

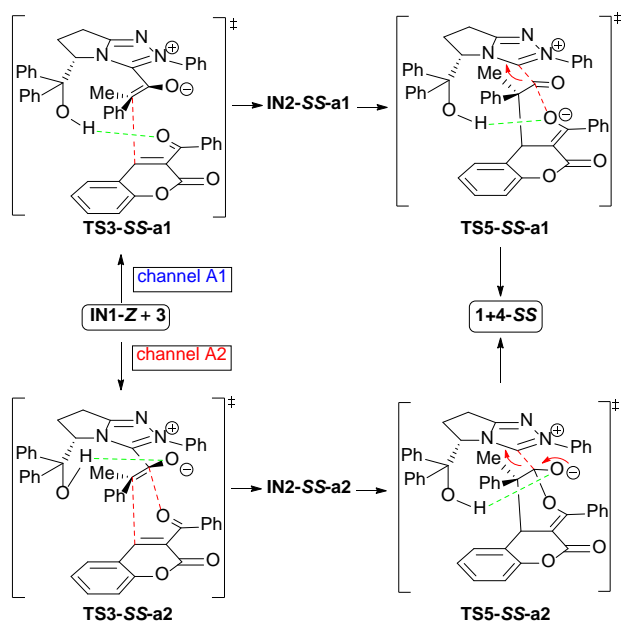
Ye and co-workers¹⁸ proposed a model for stereochemical outcome: "The enolate generated by addition of the NHC to ketene favors Z-isomer which minimizes the steric repulsion.



Scheme 5. Formation of zwitterionic intermediates **IN1-E/IN1-Z**.

The hydrogen-bonding between the hydroxy group of the NHC-ketene adduct and aryl group of the coumarin derivative directs the facial selectivity. The *endo* transition state of the Diels-Alder reaction is favored and results in the *cis*-cycloadduct observed". The transition state of the Diels-Alder reaction corresponds to the **TS2** represented in Scheme 4. However, all attempts to locate **TS2** gave disappointing results. It was possible to locate other possible reaction paths that are represented in Fig.1: channel A1, channel A2 and channel A3 (see Figure S17 of the ESI).

2.2.1 Channel A1



Scheme 6. Formation of final product 4-SS from IN1-Z and 3. Channels A1 (up) and A2 (down). Hydrogen bond in green. Bonds that are forming or breaking in red.

In this path, the intermolecular hydrogen-bonding between the hydroxyl group of the **IN1-Z** adduct and the carbonyl oxygen of benzoyl group of the coumarin **3** directs the final stereochemistry throughout the entire process (see Scheme 6 and Figures S18-S19 of the ESI). As it was shown in Scheme 6 and Fig.1, the step-by-step [4+2] cycloaddition proceeds through two elementary steps. Initially, the nucleophilic attack of enolate **IN1-Z** to the conjugate double bond of benzoyl group of the coumarin **3** (**TS3-SS-a1**) to give **IN2-SS-a1**, and finally the ring closure and simultaneous dissociation of catalyst through **TS5-SS-a1** to release the final product without going through **TS4-SS-a1** and **IN3-SS-a1** (Scheme 6 and Fig.1). This can be seen in the corresponding IRCs (see Figure S4 of the ESI). While the IRC of **TS3-SS-a1** connects the starting products **IN1-Z + 3** with the intermediate **IN2-SS-a1** (see Figure S3 of the ESI), the IRC of **TS5-SS-a1** connects the intermediate **IN2-SS-a1** with the final products **1 + 4-SS** (see Figure S4 of the ESI). The IRC of **TS5-SS-a1** also shows that part of the energy increase is due to the initial approach of O3 to carbonyl C2. In fact, in that TS the bond O3-C2 is almost formed, while the

extrusion of the NHC has barely begun (see Figure S4 of the ESI).

The Gibbs free energy barriers via **TS3-SS-a1** and **TS5-SS-a1** from **1+2+3** are 12.2 and 22.0 kcal mol⁻¹, respectively (Table S2 of the ESI), indicating that the **TS5-SS-a1** is the rate-determining step of channel A1.

2.2.2 Channel A2

In this path the hydrogen bond that directs the final stereochemistry throughout the entire process corresponds to the intramolecular hydrogen-bonding between the hydroxyl group of the **IN1-Z** adduct and the carbonyl oxygen of the original ketene group (see Scheme 6 and Figures S18-S19 of the ESI). This route may seem a priori more unfavorable since it does not facilitate the approximation of coumarin **3** to intermediate **IN1-Z**. However, as we will see later, it turned out to be less energetic than channel A1.

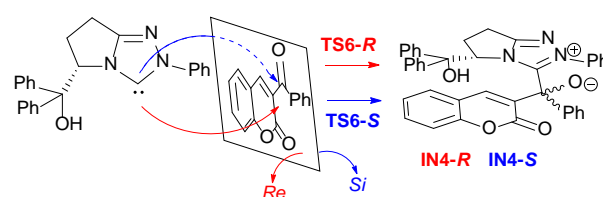
As it was shown in Scheme 6 and Fig.1, the [4+2] cycloaddition proceeds through a two stages-one step mechanism. The nucleophilic attack of enolate **IN1-Z** to the conjugate double bond of benzoyl group of the coumarin **3** (**TS3-SS-a2**) gives directly **IN3-SS-a2** without going through **IN2-SS-a2** and **TS4-SS-a2**. In intermediate **IN3-SS-a2** both bonds C1-C10b and O3-C2 are already formed. The corresponding IRC shows a totally asynchronous process, the bond O3-C2 does not start to form until the bond C1-C10b is almost formed (see Figure S5 of the ESI). In this case the hydrogen-bonding between the hydroxyl group of the **IN1-Z** adduct and the carbonyl oxygen of the original ketene group increases the nucleophilicity of this carbonyl. At the same time, the absence of the hydrogen bond between the hydroxyl group of the **IN1-Z** adduct and O3 increases the nucleophilic character of the latter (compare **TS3-SS-a1** and **TS3-SS-a2** in the Figure S19 of the ESI). This facilitates the attack of O3 to carbonyl C2. Finally, the extrusion of catalyst through **TS5-SS-a2** leads to the final product **4-SS**.

The Gibbs free energy barriers via **TS3-SS-a2** and **TS5-SS-a2** from **1+2+3** are 15.7 and 16.4 kcal mol⁻¹, respectively (Table S2 of the ESI). Both TSs have a fairly similar energy, with the free energy of **TS5-SS-a2** being slightly higher. This route is more favorable than route A1 in about 5.6 kcal mol⁻¹.

It should be noted that another channel connecting intermediate **IN2-SS-a1** to intermediate **IN3-SS-a2** was found (see channel A3, Table S2, Figures S17/S22 and Scheme S1 of the ESI). This variant does not improve the most favorable channel A2 from the energy point of view.

2.3 Mechanism B

As shown in Scheme 4 and Fig.1, mechanism B follows the

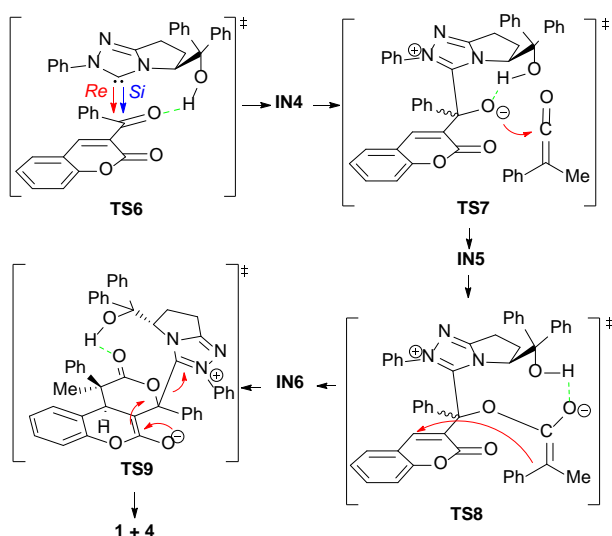


Scheme 7. Formation of zwitterionic intermediates **IN4-R/IN4-S**.

assumption that it should be the coumarin **3** that combines with the NHC catalyst in advance. There are four steps involved in mechanism B, including the nucleophilic attack of NHC **1** to coumarin **3**, then the two stepwise bonding processes of O3 atom with C2 atom and C1 atom with C10b atom, and finally release of the product and catalyst.

The first step of the reaction is the formation of zwitterionic intermediates **IN4-R/IN4-S** via nucleophilic attack of NHC **1** to the *Re* or *Si* face of coumarin **3** via the transition states **TS6-R/TS6-S** (Scheme 7). Both possibilities have been considered giving rise to channels B1 (*Re* attack) and B2 (*Si* attack). In both cases the intermolecular hydrogen-bonding between the hydroxyl group of NHC **1** and the carbonyl oxygen of benzoyl group of the coumarin **3**, facilitates the attack of the NHC (see Scheme 8 and Figures S20-S21 of the ESI).

2.3.1 Channel B1



Scheme 8. Mechanism B.

After the initial attack of NHC **1** to the *Re* face of coumarin **3** through **TS6-R** ($\Delta G = 20.3 \text{ kcal mol}^{-1}$ from **1+2+3**) to give the intermediate **IN4-R**, the next two steps are the stepwise [4+2] cycloaddition reactions. The first process of cycloaddition is initiated by the *endo* attack of zwitterion **IN4-R** to the ketene **2** through **TS7-RZ** ($\Delta G = 21.5 \text{ kcal mol}^{-1}$ from **1+2+3**) to give **IN5-RZ** (see Scheme 8). The most unfavorable *exo* attack, which would lead to the intermediate **IN5-RE** with the *E*-double bond, has been excluded in the following stages. In the **TS7-RZ** the hydrogen bond between the hydroxyl group of NHC **1** and the O3 of **3** is still maintained.

The second process of cycloaddition through **TS8-RZ** ($\Delta G = 23.1 \text{ kcal mol}^{-1}$ from **1+2+3**) involves the bonding reaction between C1 atom and C10b atom. In this stage, the stereochemistry of both carbons present in the final product is determined. In this

case, the hydrogen bond between the hydroxyl group of **1** and the carbonyl oxygen of the ketene **2** is more favorable. Finally, the catalyst **1** through **TS9-RZ** ($\Delta G = 32.4 \text{ kcal mol}^{-1}$ from **1+2+3**) is released. This last step is the rate-determining step of channel B1.

2.3.2 Channel B2

Channel B2 proceeds in a similar manner to channel B1, but passing through **TS6-S**, **TS7-SZ**, **TS8-SZ** and **TS9-SZ**. The **TS8-SZ** ($\Delta G = 26.2 \text{ kcal mol}^{-1}$ from **1+2+3**) corresponds to the rate-determining step of this channel. This route is more favorable than route B1 in about $6.2 \text{ kcal mol}^{-1}$ (compare **TS9-RZ** and **TS8-SZ**).

Taking both mechanisms discussed above (mechanism A and mechanism B) into consideration, the energy barrier of mechanism A (channel A2) is $16.4 \text{ kcal mol}^{-1}$ for the rate-determining step via **TS5-SS-a2** while it is $26.2 \text{ kcal mol}^{-1}$ for mechanism B (channel B2) via **TS8-SZ**.

2.4 MPWB1K/6-311G** in toluene // B3LYP/6-31G* in gas-phase for channel A2 and channel B2.

In order to ensure that the conclusions drawn at B3LYP/6-31G* level are valid at different levels of calculation, single-point calculations at MPWB1K/6-311G** level in toluene, were made of the species involved in channel A2 and channel B2.

The free energy profiles are shown in Fig.2 (see also Table S4 of the ESI for a more detail of the energies).

There are notable changes in the energies of the species. An increase of stability is especially pronounced in **TS3-SS-a2** / **TS5-SS-a2** (channel A2) and **TS8-SZ** / **TS9-SZ** (channel B2). As a result of these changes, **TS1-S** ($\Delta G = 19.4 \text{ kcal mol}^{-1}$ from **1+2+3**) become the rate-determining step of channel A2 and **TS6-Z** ($\Delta G = 22.9 \text{ kcal mol}^{-1}$ from **1+2+3**) become the rate-determining step of channel B2. We can conclude that mechanism A (channel A2) is more energetically favorable.

It should be noted that **TS8-SZ** determines the stereochemistry of the final products (**4-SS**) through mechanism B (channel B2). The **TS8-enant** (see table S4 and Figure S21 of the ESI) was also calculated. This would give rise to **4-RR** which is the enantiomeric form obtained experimentally in smaller proportion. The result is that its energy ($\Delta G = 8.2 \text{ kcal mol}^{-1}$ from **1+2+3**) is lower than that obtained for the **TS8-SZ** ($\Delta G = 11.3 \text{ kcal mol}^{-1}$ from **1+2+3**) and would lead to a greater proportion of the final product **4-RR** versus **4-SS**. This result does not fit the experimental result and is an additional circumstance to rule out mechanism B versus mechanism A.

In this way, the first two questions are resolved: a) What is the possible mechanism? : “ketene-first” mechanism A b) What is the possible detailed mechanism?: mechanism A (channel A2).

The third question would remain: c) Is it possible to predict the final stereochemistry?

2.5 Prediction of enantioselectivity

In order to determine the enantiomeric excess observed experimentally, we carried out a detailed theoretical study at a high level and with solvent effect. The selected mechanism corresponds to the most favorable channel A2 from the energy point of view. We studied the two routes that lead to both enantiomers, mechanism A2-SS (corresponding to mechanism A2 previously studied) and mechanism A2-RR (variation of the A2 mechanism leading to the 4-RR enantiomer). Species involved in this mechanism were optimized in toluene, using

involved in mechanism A2-SS (compare **TS1-Z**, **TS3-SS-a2** and **TS5-SS-a2** in Figures S18-S19 with the same TSs in Figure S23 of the ESI). However, there are notable changes in the energies of the species. An increase of stability of all the species with respect to **1+2+3** is observed. This increase in stability is especially pronounced in **TS3-SS-a2**, **IN3-SS-a2**, **TS5-SS-a2** and **1-4-SS**. While **TS1-Z**, **TS3-SS-a2** and **TS5-SS-a2** at B3LYP/6-31G* level have similar energies ($\Delta G = 16.2, 15.7$ and $16.4 \text{ kcal mol}^{-1}$, respectively). See Fig. 1), these same transition states at

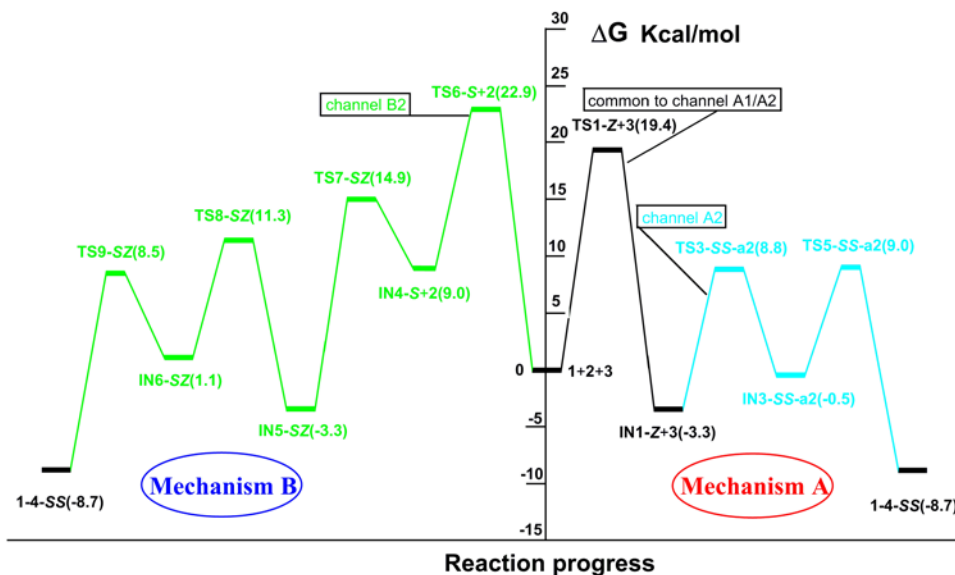


Fig.2 Free energy profiles, at MPWB1K/6-311G**, in toluene//B3LYP/6-31G*, in gas phase, of channel A2 (in blue) and channel B2 (in green).

the MPWB1K/6-311G** level. This level of theory has shown to have good results for combinations of thermochemistry and thermochemical kinetics in processes including weak interactions. The relative energies (ΔG) associated with the conversion of **1+2+3** into **4-SS** and **4-RR** are given in Fig. 3 (see also Tables S5-S6 of the ESI). The geometries are shown in Figure S23 of the ESI.

The inclusion of the solvent and the MPWB1K/6-311G** level, does not produce significant geometric changes in species

MPWB1K/6-311G** level have different energies ($\Delta G = 15.4, -3.6$ and $-5.7 \text{ kcal mol}^{-1}$, respectively). See Fig. 3).

The reaction path that starts from the **IN1-Z** and leads to the enantiomer **4-RR** (mechanism A2-RR in Fig. 3), is similar to that found for the enantiomer **4-SS** (mechanism A2-SS in Fig. 3). The transition states **TS3-RR-a2** and **TS5-RR-a2** have relative energies (ΔG) of -0.8 and $-8.6 \text{ kcal mol}^{-1}$, respectively (see Fig. 3). These relative energies are similar to the relative energies of transition states **TS3-SS-a2** and **TS5-SS-a2**. As seen in Fig. 3, the rate-determining step for the conversion of intermediate **IN1-Z** (common to both mechanisms) in the final products **4-SS** and **4-RR** corresponds to the transition states **TS3-SS-a2** and **TS3-RR-a2**, respectively. It should be noted that these transition states determine the stereochemistry of the final products and therefore correspond to the enantioselectivity-determining step. The transition state **TS3-SS-a2** is $2.8 \text{ kcal mol}^{-1}$ more stable than the transition state **TS3-RR-a2**. These results are in agreement with the experimental outcome of 87% ee.¹⁸

What is the origin of stereoselectivity ?

If we observe the structure of **TS3-SS-a2** and **TS3-RR-a2** (see Figure S23 of the ESI) there are two main causes that facilitate their stabilization: hydrogen-bonding and π - π -stacking. In both cases there is an intramolecular hydrogen-bonding between the hydroxyl group of the **IN1-Z** adduct and the carbonyl oxygen of the original ketene group. This hydrogen-bonding

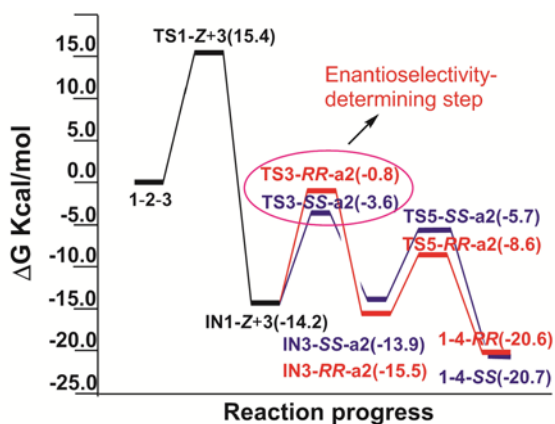


Fig.3 Free energy profiles (ΔG) of mechanism A2 at MPWB1K/6-311G** level, in toluene. Mechanism A2-SS isomer (in blue) and mechanism A2-RR isomer (in red).

does not seem to be the main cause of the energy difference between the two TSs. The distance H...O in **TS3-SS-a2** is 2.291 Å and 1.871 Å in **TS3-RR-a2**. The smaller distance in the **TS3-RR-a2** apparently would favour the greater stabilization of **TS3-RR-a2** compared to **TS3-SS-a2**. It must be the stabilization produced by π - π -stacking the origin of the stereoselectivity.² Although both transition states show π - π -stacking between the aromatic ring of chromenone and the aromatic ring on the triazole fragment, there are differences. In **TS3-SS-a2**, the distance between both aromatic rings is 4.002 Å and the dihedral angle between the aromatic rings is 29.9° (ideally it would be 0°). For **TS3-RR-a2** these measures are 4.140 Å and 31.5°. The stabilization due to π - π -stacking in **TS3-SS-a2** is superior to that of **TS3-RR-a2**.

In view of these results, the NHC can be modified to change the ratio between the final stereoisomers: it is quite reasonable to think that the presence of substituents other than hydrogen on the aromatic ring over the triazole fragment, can modify the π - π -stacking and therefore the energy and proportion between the **TS3-SS** and **TS3-RR**.

3-Summary and Conclusions

A theoretical study of the NHC-catalysed enantioselective cycloaddition of ketenes and 3-aryl coumarins to give the corresponding dihydrocoumarin-fused multisubstituted dihydropyranones has been carried out.

Initially, at B3LYP/6-31G* level in gas phase, two possible mechanisms have been studied:

-1. "Ketene-first" mechanism A. In this mechanism the nucleophilic catalyst initially attacks the ketene to generate a NHC-ketene zwitterionic intermediate, which is followed by reaction between this enolate and the aryl coumarin, cyclization and expulsion of NHC close the reaction pathway.

-2. "Coumarin-first" mechanism B. In this mechanism the nucleophilic catalyst initially attacks the aryl coumarin to generate a NHC-aryl coumarin intermediate. This intermediate attacks to the ketene and after expulsion of NHC gives the final product.

We can conclude that mechanism A, through channel A2, is more favorable. The first step of the reaction is the formation of zwitterionic intermediate **IN1-Z** via nucleophilic attack of NHC **1** to ketene **2** via the transition state **TS1-Z**. The second step is the [4+2] cycloaddition which takes place through a two stage-one step mechanism. In this step nucleophilic attack of enolate **IN1-Z** to the conjugate double bond of benzoyl group of the coumarin **3**, through **TS3-SS-a2**, yield **IN3-SS-a2**. Finally, the extrusion of catalyst through **TS5-SS-a2** leads to the final product **4-SS**. In this path the hydrogen bond, that directs the final stereochemistry throughout the entire process, corresponds to the intramolecular hydrogen-bonding between the hydroxyl group of the **IN1-Z** adduct and the carbonyl oxygen of the original ketene group.

The theoretical studies, carried out at MPWB1K/6-31G** level in toluene, indicate that the origin of the enantioselectivity observed in the experimental results is determined in the transition states **TS3-SS-a2**/ **TS3-RR-a2**.

The most probable cause of the origin of stereoselectivity is the π - π -stacking between the aromatic ring of chromenone and the aromatic ring on the triazole fragment in **TS3**. From the experimental point of view, the modification of the substituents in the aromatic ring over the triazole fragment of the NHC, can alter the proportion between the final stereoisomers.

Conflicts of interest

There are no conflicts to declare.

Acknowledgements

This study was supported by intramural grant 201680I008 from the Spanish Government (Consejo Superior de Investigaciones Científicas).

References

- 1 D. M. Flanigan, F. Romanov-Michailidis, N. A. White and T. Rovis, *Chem. Rev.*, 2015, **115**, 9307.
- 2 Y. Wang, D. Wei, and W. Zhang, *ChemCatChem*, 2018, **10**, 338.
- 3 J. Mahatthananchai and J. W. Bode, *Acc. Chem. Res.*, 2014, **47**, 696.
- 4 X. Bugaut and F. Glorius, *Chem. Soc. Rev.*, 2012, **41**, 3511.
- 5 Y.-R. Zhang, H. Lv, D. Zhou and S. Ye, *Chem. Eur. J.*, 2008, **14**, 8473.
- 6 X.-L. Huang, L. He, P.-L. Shao and S. Ye, *Angew. Chem., Int. Ed.*, 2009, **48**, 192.
- 7 Y.-R. Zhang, L. He, X. Wu, P.-L. Shao and S. Ye, *Org. Lett.*, 2008, **10**, 277.
- 8 N. Duguet, C. D. Campbell, A. M. Z. Slawin and A. D. Smith, *Org. Biomol. Chem.*, 2008, **6**, 1108.
- 9 D. Wei, Y. Zhu, C. Zhang, D. Sun, W. Zhang and M. Tang, *J. Mol. Catal. A: Chem.*, 2011, **334**, 108.
- 10 M. Zhang, D. Wei, Y. Wang, S. Li, J. Liu, Y. Zhu and M. Tang, *Org. Biomol. Chem.*, 2014, **12**, 6374.
- 11 X.-N. Wang, L.-T. Shen and S. Ye, *Org. Lett.*, 2011, **13**, 6382.
- 12 X.-N. Wang, H. Lv, X.-L. Huang and S. Ye, *Org. Biomol. Chem.*, 2009, **7**, 346.
- 13 X.-N. Wang, L.-T. Shen and S. Ye, *Chem. Commun.*, 2011, **47**, 8388.
- 14 J. Douglas, K. B. Ling, C. Concellón, G. Churchill, A. M. Z. Slawin and A. D. Smith, *Eur. J. Org. Chem.*, 2010, 5863.
- 15 K. Tang, J. Wang, X. Cheng, Q. Hou and Y. Liu, *Eur. J. Org. Chem.*, 2010, 6249.
- 16 W. Zhang, Y. Zhu, D. Wei, Y. Li and M. Tang, *J. Org. Chem.*, 2012, **77**, 10729.
- 17 Y. Ran, M. Tang, Y. Wang, Y. Wang, X. Zhang, Y. Zhu, D. Wei and W. Zhang, *Tetrahedron*, 2016, **72**, 5295.
- 18 T.-Y. Jian, X.-Y. Chen, L.-H. Sun and S. Ye, *Org. Biomol. Chem.*, 2013, **11**, 158.
- 19 (a) M. J. Aurell, L. R. Domingo, M. Arnó and R. J. Zaragoza, *Org. Biomol. Chem.*, 2016, **14**, 8338; (b) L. R. Domingo, R. J. Zaragoza and M. Arnó, *Org. Biomol. Chem.*, 2011, **9**, 6616; (c) L. R. Domingo, R. J. Zaragoza and M. Arnó, *Org. Biomol. Chem.*, 2010, **8**, 4884.
- 20 M. J. Frisch, et al., *Gaussian 09, Revision A.02*, Gaussian, Inc., Wallingford, CT, 2009.
- 21 (a) R. G. Parr and W. Yang, *Density Functional Theory of Atoms and Molecules*, Oxford University Press, New York, 1989; (b) T. Ziegler, *Chem. Rev.*, 1991, **91**, 651.

- 22 (a) A. D. Becke, *J. Chem. Phys.*, 1993, **98**, 5648; (b) C. Lee, W. Yang and R. G. Parr, *Phys. Rev. B*, 1988, **37**, 785.
- 23 W. J. Hehre, L. Radom, P. von R. Schleyer and J. A. Pople, *Ab initio Molecular Orbital Theory*, Wiley, New York, 1986.
- 24 K. Fukui, *J. Phys. Chem.*, 1970, **74**, 4161.
- 25 (a) C. González and H. B. Schlegel, *J. Phys. Chem.*, 1990, **94**, 5523; (b) C. González and H. B. Schlegel, *J. Chem. Phys.* 1991, **95**, 5853.
- 26 Y. Zhao and D. G. Truhlar, *J. Phys. Chem. A*, 2004, **108**, 6908.
- 27 (a) J. Tomasi and M. Persico, *Chem. Rev.*, 1994, **94**, 2027; (b) B. Y. Simkin, I. Sheikhet, *Quantum Chemical and Statistical Theory of Solutions-A Computational Approach*, Ellis Horwood, London, 1995.
- 28 (a) E. Cancès, B. Mennucci and J. Tomasi, *J. Chem. Phys.*, 1997, **107**, 3032; (b) M. Cossi, V. Barone, R. Cammi and J. Tomasi, *Chem. Phys. Lett.* 1996, **255**, 327; (c) V. Barone, M. Cossi and J. Tomasi, *J. Comp. Chem.*, 1998, **19**, 404.